Resonant diffraction mechanism, nonreciprocity, and lock-in in the ring-laser gyroscope

Fabien Bretenaker,* Bruno Lépine,† Annie Le Calvez,‡ Olivier Adam,‡ Jean-Paul Taché, and Albert Le Floch
Laboratoire d'Electronique Quantique-Physique des Lasers, Université de Rennes I, Campus de Beaulieu, F-35042 Rennes CEDEX, France
(Received 17 June 1992)

Diffraction is shown to play a dramatic role in the frequency characteristics of ring-laser gyroscopes. It is proved theoretically and experimentally that a small misalignment of the cavity leads to a nonreciprocity of the resonant diffraction mechanism. The resonant diffraction losses of the two counterpropagating modes being then different, the asymmetries of their output-power versus cavity-frequency profiles are different. This leads to the existence of a frequency bias between the two modes. Diffraction is also shown to play a fundamental role in the lock-in mechanism. It is indeed experimentally demonstrated that the asymmetric evolution of the lock-in threshold with the laser frequency is governed by resonant diffraction mechanisms.

PACS number(s): 42.60.Da, 42.60.Jf, 42.25.Fx

I. INTRODUCTION

The main difference between ring lasers and usual Fabry-Pérot cavity lasers is the possibility to sustain the oscillation of traveling waves rather than standing waves. This has led to many applications, such as, for instance, the use of unidirectional ring lasers to cancel the spatial hole burning due to the nodes and antinodes of the standing waves in order to obtain more important powers or to increase the coupling between the different longitudinal modes of the laser [1]. A very important application of bidirectional ring lasers is their use as inertial rotation sensors in ring-laser gyroscopes (RLG's) [2–4]. In such devices, the rotation leads to a path-length difference between the two counterpropagating paths, known as the Sagnac effect [5]. This induces a frequency difference between the two counterpropagating modes that is directly proportional to the angular velocity of the cavity. The main problems in these devices are the *null shift* and the *lock-in region* [4]. The null shift consists in a rotation-independent nonreciprocity that is a major error source in the RLG. A possible mechanism to explain this null shift is based on Langmuir flows present in the active medium that induce nonreciprocities via Fresnel drag [6]. This effect is compensated by building cavities admitting a plane of symmetry with two symmetrical gas discharges. Null-shift errors are also observed when the aperture that selects the TEM_{00} fundamental Gaussian mode of the cavity is not located in the plane of symmetry of the cavity and is misaligned [7–10]. This effect has been investigated theoretically for hard [11–15] or Gaussian apertures [16–21]. The lock-in region is a frequency locking of the two counterpropagating modes that occurs for values of the angular rotation rate Ω smaller than a value Ω_{LI}, called lock-in threshold. This effect is attributed to the mirror defects that create a coupling between the two counterpropagating modes of the laser [4,22]. However, some aspects of the physics of the lock-in region have not yet been clearly explained, such as the asymmetry of its evolution with the mean frequency detuning of the laser [23]. Besides, recently, the cause of the asymmetries of the output-power versus frequency profiles in ring lasers has been isolated [24]. It has been shown that these asymmetries are due to the frequency-dependent lenslike effects that exist in the active medium. These lenslike effects have been shown to induce frequency-dependent variations of the tangential and sagittal sizes of the elliptical Gaussian mode at the location of the diffracting aperture. This mechanism induces a *dependence of diffraction losses with frequency* that creates the observed asymmetries. This dynamics has been described theoretically using the *ABCD* matrix formalism [25] in the sagittal (perpendicular to the cavity) and tangential (parallel to the cavity) planes. The concepts of short (long) cavities in the sagittal and tangential planes have been isolated, for which a convergent lenslike effect leads to a decrease (increase) of the mode size at the aperture and of the diffraction losses [24]. The cases of tangential or sagittal critical geometries have been predicted and observed, for which the tangential or sagittal mode size at the aperture is independent of the lenslike effect. A fully critical geometry which is critical in both planes simultaneously has also been isolated. This mode-size dynamics has been investigated for different types of lenslike effects and different isotopic compositions of the active medium [26]. This permits one to understand the observed asymmetries for any ring laser. However, these effects have been investigated for ring lasers at rest, when the two counterpropagating modes have the same frequency and can consequently be treated as a unique standing wave with a good approximation. The aim of this paper is consequently to explore the influence of the resonant diffraction mechanisms on the frequency characteristics of the RLG. In the first part, we show theoretically and experimentally how the resonant diffraction-losses mechanism studied in Refs. [24,26] can become nonreciprocal and induce a null shift. In the second part, we show, as partly pointed out in Ref. [27], that diffraction can play an important role in the lock-in mechanism.

II. NONRECIPROCITY OF THE RESONANT DIFFRACTION LOSSES MECHANISM

A. Theory

1. Diffraction of a Gaussian beam by a misaligned aperture

To introduce the physics of nonreciprocity in the ring laser, let us consider a circular Gaussian beam produced by a commercial 6328-Å He-Ne laser with mode size $w=932$ μm and wave-front radius of curvature $R=1.84$ m. This beam is incident on a circular aperture of diameter $\phi=2$ mm whose center is slightly translated in the horizontal plane perpendicularly to the beam axis of $a=0.25$ mm [see Fig. 1(a)]. The resulting power profiles obtained by scanning a small-size detector in the horizontal plane at a distance d behind the aperture are shown in Fig. 1(a) for $d=0.12$ and 0.9 m. We can see that just behind the aperture the beam appears to be truncated and that its shape evolves along its further propagation. One can calculate the resulting beam thanks to the Huyghens-Fresnel principle [28]. The transverse dependence of the electric field associated with the incident beam can be written

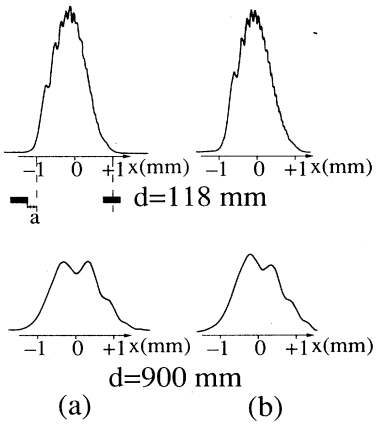

FIG. 1. (a) Experimental and (b) theoretical intensity profiles of a Gaussian beam diffracted by a slightly misaligned aperture, observed at two different distances behind the aperture [the misaligned aperture is schematized in (a)].

$$u_1(x,y)=\frac{w_0}{w}\exp[-i\frac{k}{2R}(x^2+y^2)]\exp\left[-\frac{x^2+y^2}{w^2}\right], \tag{1}$$

where z is the propagation direction and x the horizontal axis. $k=2\pi/\lambda$ is the wave number and w_0 the beam waist. The electric-field distribution at distance d behind the aperture can be written

$$u_2(x,y)=\frac{i}{\lambda d}e^{-ikd}\int\int_{\text{aperture}}u_1(x_1,y_1)e^{-(ik/2d)[(x-x_1)^2+(y-y_1)^2]}dx_1dy_1\ . \tag{2}$$

This calculation can be simplified in approximating the aperture by a stripe of width ϕ located in $x=a$. Then, keeping only the field dependence along x and z, the incident field can be written

$$u_1(x)=\left[\frac{w_0}{w}\right]^{1/2}\exp\left[-i\frac{kx^2}{2R}\right]\exp\left[-\left[\frac{x}{w}\right]^2\right]. \tag{3}$$

The detected field is then approximately given by

$$u_2(x)=\frac{i}{\sqrt{\lambda d}}e^{-ikd}\times\int_{a-\phi/2}^{a+\phi/2}u_1(x_1)\exp\left[-i\frac{k}{2d}(x-x_1)^2\right]dx_1\ . \tag{4}$$

The results of this calculation are shown in Fig. 1(b) and are in good agreement with the experimental results. These results show that when a Gaussian beam is diffracted by a misaligned aperture, its shape evolves along its propagation. In particular, the curvature of its transverse intensity profile evolves very quickly.

2. Nonreciprocity of the resonant diffraction: Theory

Let us now consider the ring cavity schematized in Fig. 2. It is built with a spherical mirror and two plane mirrors. The active medium is located in a symmetric manner with respect to the mirrors. Let us introduce a diffracting aperture in D_1 and no aperture in D_2. Then, the path length from the aperture to the active medium is longer for the counterclockwise (CCW) wave than for the clockwise (CW) wave. If the aperture is slightly misaligned, the results of Sec. II A 1 show that the two distorted beams will not have the same transverse intensity profiles inside the active medium any more. As the so-called saturation lenslike effect undergone by one

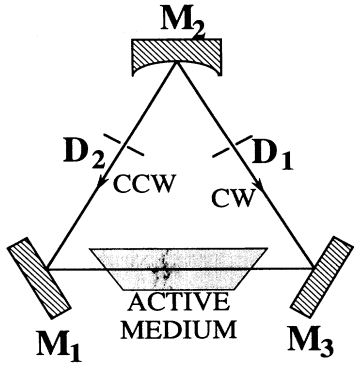

FIG. 2. Considered ring cavity. Notice the two possible positions of the diffracting aperture, labeled D_1 and D_2.

mode is due to the transverse inhomogeneity of the saturation of its refractive index by the other mode [29,30], the two modes will not undergo the same variations of the mode sizes at the aperture any more. Consequently the resonant diffraction losses and *the asymmetries of the output-power versus frequency profiles will not be equal for the two modes* anymore. The Lamb equations that describe the evolutions of the intensities and angular frequencies of the two modes can then be written, without taking lock-in mechanisms into account [1]:

$$\dot{I}_{\mathrm{CW}}=2I_{\mathrm{CW}}(\alpha_{\mathrm{CW}}-\beta_{\mathrm{CW}}I_{\mathrm{CW}}-\delta p_{\mathrm{CW}}I_{\mathrm{CCW}} -\theta_{\mathrm{CW\text{-}CCW}}I_{\mathrm{CCW}}) , \tag{5}$$

$$\dot{I}_{\mathrm{CCW}}=2I_{\mathrm{CCW}}(\alpha_{\mathrm{CCW}}-\beta_{\mathrm{CCW}}I_{\mathrm{CCW}}-\delta p_{\mathrm{CCW}}I_{\mathrm{CW}} -\theta_{\mathrm{CCW\text{-}CW}}I_{\mathrm{CW}}) , \tag{6}$$

$$\omega_{\mathrm{CW}}+\dot{\phi}_{\mathrm{CW}}=\Omega_{\mathrm{CW}}+\sigma_{\mathrm{CW}}-\rho_{\mathrm{CW}}I_{\mathrm{CW}}-\tau_{\mathrm{CW\text{-}CCW}}I_{\mathrm{CCW}} , \tag{7}$$

$$\omega_{\mathrm{CCW}}+\dot{\phi}_{\mathrm{CCW}}=\Omega_{\mathrm{CCW}}+\sigma_{\mathrm{CCW}}-\rho_{\mathrm{CCW}}I_{\mathrm{CCW}}-\tau_{\mathrm{CCW\text{-}CW}}I_{\mathrm{CW}} , \tag{8}$$

where I_{CW} and I_{CCW} are the intensities of the two modes, ω_{CW} and ω_{CCW} their angular frequencies, ϕ_{CW} and ϕ_{CCW} their phases, α_{CW} and α_{CCW} their unsaturated net gains per second, β_{CW} and β_{CCW} their self-saturation coefficients, and $\theta_{\mathrm{CW\text{-}CCW}}$ and $\theta_{\mathrm{CCW\text{-}CW}}$ their cross-saturation coefficients. Ω_{CW} and Ω_{CCW} are the resonance pulsations of the empty cavity, σ_{CW} and σ_{CCW} are the pulling coefficients, ρ_{CW} and ρ_{CCW} the self-pushing coefficients, and $\tau_{\mathrm{CW\text{-}CCW}}$ and $\tau_{\mathrm{CCW\text{-}CW}}$ the cross-pushing coefficients. With respect to the usual Lamb's equations, we have added the two terms $\delta p_{\mathrm{CW}}I_{\mathrm{CCW}}$ and $\delta p_{\mathrm{CCW}}I_{\mathrm{CW}}$ inside Eqs. (5) and (6) to take the resonant diffraction mechanism into account. Indeed, the resonant diffraction losses undergone by one mode are due to the saturation lenslike effect induced by the other one and consequently evolve like the square of the field, like the cross-pushing term. Thus we can see that this resonant diffraction-losses term is a competitionlike term, i.e., a cross-saturation-like term. Hence, we can define modified cross-saturation coefficients that allow one to rewrite Lamb's equations in their original shape:

$$\theta'_{\mathrm{CW\text{-}CCW}}=\theta_{\mathrm{CW\text{-}CCW}}+\delta p_{\mathrm{CW}} , \tag{9a}$$

$$\theta'_{\mathrm{CCW\text{-}CW}}=\theta_{\mathrm{CCW\text{-}CW}}+\delta p_{\mathrm{CCW}} . \tag{9b}$$

One can then define a new coupling constant between the two modes:

$$C=\frac{\theta'_{\mathrm{CW\text{-}CCW}}\theta'_{\mathrm{CCW\text{-}CW}}}{\beta_{\mathrm{CW}}\beta_{\mathrm{CCW}}} . \tag{10}$$

The expressions of the different Lamb's coefficients are summarized in the Appendix for the case of an inhomogeneously broadened single-isotope active medium. Concerning the resonant diffraction-losses coefficient, its evolution with frequency is identical to the one of the saturation lenslike effect [30,31], i.e., the dispersion curve associated with the homogeneous broadening of the transition:

$$\delta p_{\mathrm{CW}}=\delta B_{\mathrm{CW}}\frac{\gamma\nu_{\mathrm{CW}}}{\gamma^2+\nu_{\mathrm{CW}}^2} , \tag{11a}$$

$$\delta p_{\mathrm{CCW}}=\delta B_{\mathrm{CCW}}\frac{\gamma\nu_{\mathrm{CCW}}}{\gamma^2+\nu_{\mathrm{CCW}}^2} , \tag{11b}$$

where γ is the homogeneous width of the transition and ν the mean frequency detuning of the two modes with respect to the transition center frequency. The coefficients δB_{CW} and δB_{CCW} are positive (negative) for a short (long) cavity, i.e., a cavity for which a convergent lenslike effect reduces (increases) the size of the mode at the aperture. The stationary regime intensities for the case $C<1$ (weak coupling) are given by

$$I_{\mathrm{CW}}=\frac{\alpha_{\mathrm{CW}}-\theta'_{\mathrm{CW\text{-}CCW}}\dfrac{\alpha_{\mathrm{CCW}}}{\beta_{\mathrm{CCW}}}}{\beta_{\mathrm{CW}}(1-C)} , \tag{12a}$$

$$I_{\mathrm{CCW}}=\frac{\alpha_{\mathrm{CCW}}-\theta'_{\mathrm{CCW\text{-}CW}}\dfrac{\alpha_{\mathrm{CW}}}{\beta_{\mathrm{CW}}}}{\beta_{\mathrm{CCW}}(1-C)} , \tag{12b}$$

For a ring laser at rest and a null shift negligible compared to γ, one has $\Omega_{\mathrm{CW}}\approx\Omega_{\mathrm{CCW}}$, $\sigma_{\mathrm{CW}}\approx\sigma_{\mathrm{CCW}}$, $\tau_{\mathrm{CW\text{-}CCW}}\approx\tau_{\mathrm{CCW\text{-}CW}}=\tau$, and also $\rho_{\mathrm{CW}}=\rho_{\mathrm{CCW}}=0$ for traveling waves [1]. Then, the frequency difference between the two modes becomes

$$\Delta\nu=\frac{1}{2\pi}[(\omega_{\mathrm{CCW}}+\dot{\phi}_{\mathrm{CCW}})-(\omega_{\mathrm{CW}}+\dot{\phi}_{\mathrm{CW}})] =\frac{\tau}{2\pi}(I_{\mathrm{CW}}-I_{\mathrm{CCW}}) . \tag{13}$$

If the aperture is misaligned, then $\delta B_{\mathrm{CW}}\neq\delta B_{\mathrm{CCW}}$ so that $I_{\mathrm{CW}}\neq I_{\mathrm{CCW}}$. Equation (13) shows consequently that $\Delta\nu\neq 0$: a null shift appears. Figure 3 represents the evolution of such a null shift with respect to the mean frequency detuning of the two modes for a relative excitation $\eta=1.3$, $\gamma=50$ MHz and for $\delta B_{\mathrm{CCW}}>\delta B_{\mathrm{CW}}>0$. In this case the output-power versus frequency profile of the CCW mode is more asymmetric than that of the CW mode and both modes exhibit the same kind of asymmetry: The output power is more important on the low-frequency side of the transition than on the high-frequency side. The intensity difference I_{CW}-I_{CCW} is con-

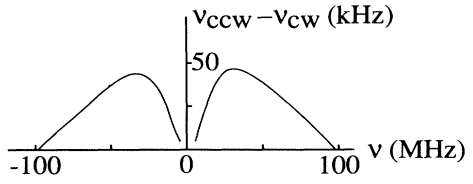

FIG. 3. Calculated evolution of the null shift vs cavity detuning. The cavity is supposed to be short in both planes and the lenslike effect undergone by the CCW mode stronger than the one undergone by the CW mode.

sequently negative on the low-frequency side and positive on the high-frequency side of the transition. As the coefficient τ is also negative on the low-frequency side and positive on the high-frequency side of the transition [see the Appendix, Eq. (A6)], the frequency difference $\Delta\nu$ is always positive. *For a short (long) cavity, the mode with the higher frequency is consequently the one which exhibits the more (less) asymmetric power profile.* The curve of Fig. 3 exhibits a zero at the center of the profile. This is due to the fact that $\tau=0$ at the center of the transition. Obviously, if one removes the aperture D_1 from the cavity of Fig. 2 and introduces the aperture D_2 and misaligns it in a symmetrical manner, the roles of the two modes are exchanged in the preceding results. In particular, the null shift $\Delta\nu$ must change sign.

B. Experimental results

The experimental setup used to test the predictions of Sec. II A is schematized in Fig. 4. The laser oscillates at $\lambda=3.39$ μm and the active medium is a 5:1 ^{3}He-^{20}Ne gas mixture at total pressure $P=1$ Torr. The discharge tube is 30 cm long with a 6-mm bore diameter. Such a large bore diameter allows us to select the saturation lenslike effects [31]. The spherical mirror M_2 has a radius of curvature $R=2$ m and the perimeter of the cavity is 1.2 m. Mirrors M_2 and M_3 are totally reflecting and mirror M_1 transmits 10% of the incident intensity. The two output beams are recombined on the detector by mirror M_4 and the beamsplitter. Mirror M_4 can be translated perpendicularly to its plane, in order to determine the sign of the observed beating, by using the Doppler frequency shift undergone by the CCW beam due to the movement of M_4. The circular apertures used in D_1 and D_2 have diameters equal to 2.6 mm. Such a cavity is short in both the tangential and sagittal planes [24]. The observation of the intensity collected by the detector with respect to the cavity length scanned by a piezoelectric transducer gives the result reproduced in Fig. 5 when the aperture is misaligned by a fraction of a millimeter. One can see that the two counterpropagating modes do not have the same frequency anymore. Let us then observe the output-power versus frequency profiles for the two counterpropagating modes when the aperture is aligned and misaligned successively. The results are reproduced in Fig. 6. Figure 6(a) displays these profiles when the aperture is located in D_1 and is well centered on the beam. The two profiles then exhibit similar asymmetries that show that, as expected, the cavity is short and the saturation lenslike effect is predominant. In this case no frequency difference is observed when the two output beams are recombined. By slightly shifting the aperture perpen-

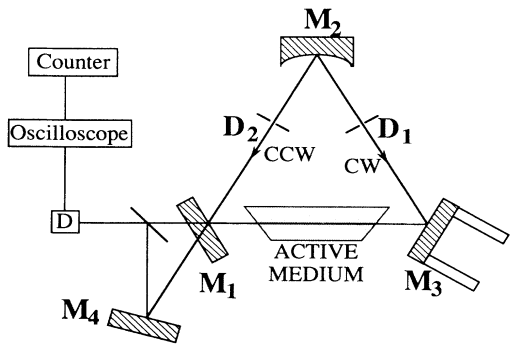

FIG. 4. Experimental setup used to observe the nonreciprocity of resonant diffraction.

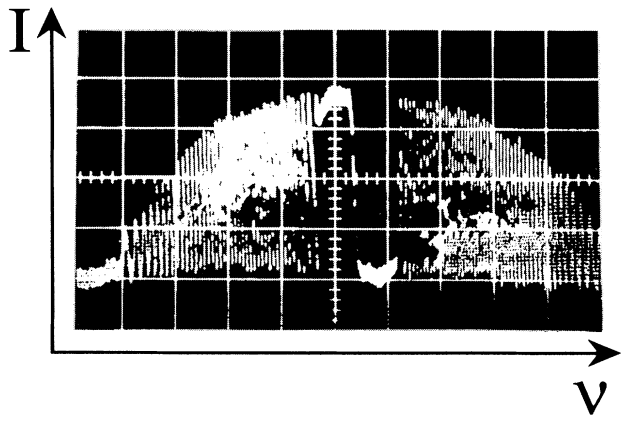

FIG. 5. Typical experimental output-power vs cavity-detuning profile obtained when the aperture is misaligned and the two modes are recombined on the detector.

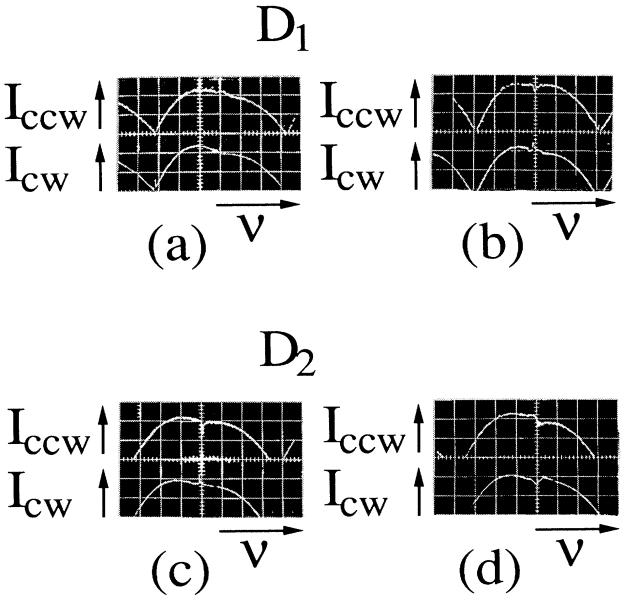

FIG. 6. Experimental observations of the evolution of the intensities of the two modes vs cavity detuning. The aperture is successively located in D_1 [(a), (b)] and in D_2 [(c), (d)]. When the aperture is centered on the beam [(a), (c)], the asymmetries of the profiles of the two modes are identical and no null shift is observed. On the contrary, when the aperture is misaligned [(b), (d)], the asymmetries of the profiles are different for the two modes and a null shift appears. One observes that the mode with the larger asymmetry has the higher frequency (see Fig. 7).

dicularly to the beam one obtains the profiles of Fig. 6(b). By moving mirror M_4 one can see that $\nu_{CW} > \nu_{CCW}$ all over the profile. This is in agreement with the fact that the output-power profile of the CW mode is much more asymmetric than that of the CCW mode. By locating the aperture in D_2 and misaligning it in a symmetrical manner, one obtains the results displayed in Figs. 6(c) and 6(d). This time, the mode with the more asymmetric profile is in the CCW one [see Fig. 6(d)] and one has $\nu_{CCW} > \nu_{CW}$. One can also check that the frequency difference disappears when the two apertures are inside the cavity with the same misalignments. By slowly scanning the cavity length one can measure the evolution of the optical beat frequency with respect to the mean detuning of the two modes. The results for the two positions of the aperture are reproduced in Fig. 7 for a relative excitation $\eta = 1.45$. The result is in good agreement with the theoretical calculation of Fig. 3. As expected, one can in particular notice that the null shift is more important on the high-frequency side of the transition for a short cavity laser.

We have consequently given theoretical and experimental evidence for the nonreciprocity of the mechanism of resonant diffraction losses. This mechanism is, in summary, the following one. If the aperture that selects the TEM_{00} elliptical Gaussian beam of a ring laser is misaligned and is not located in a plane of symmetry of the laser, the residual deformations of the two counterpropagating beams in the active medium are different. Consequently, the saturation lenslike effects that the two modes induce on each other are not identical. Thus the asymmetries of the output-power versus frequency profiles of the two modes are different, leading to different intensities for the two modes. This induces a null shift because of the cross-pushing mechanisms. One of the main characteristics of this null shift is that *its sign remains constant* for any cavity detuning, as predicted in Sec. II A and already observed in previous experiments [7–10]. This is incompatible with the nonreciprocal losses effects due to the empty cavity discussed in Refs. [32–36]. Indeed, in this case, the difference $I_{CW} - I_{CCW}$ would not change sign with the detuning and the null shift would change sign with τ, as shown in Eq. (13). The discussion in Refs. [32–36] originated from a fundamental error in Refs. [32–33]. The mechanism put into evidence here is different from the ones investigated theoretically in Refs. [11–15] and from the ones predicted in the case of Gaussian apertures [16–21]. Indeed, these references do not take into account the resonant diffraction-losses mechanism which explains the asymmetries of the output-power versus frequency profiles and whose nonreciprocity explains the null shifts observed here.

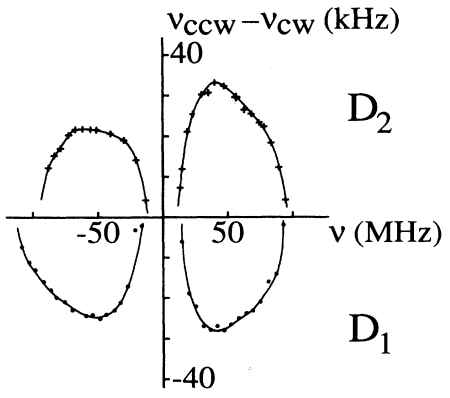

FIG. 7. Experimental measurements of the null shift vs cavity detuning for the two positions D_1 and D_2 of the misaligned aperture.

III. DIFFRACTION AND LOCK-IN MECHANISM

As already stated in the Introduction, experimental works on RLG's show that the lock-in threshold Ω_{LI} depends strongly on the detuning of the laser [2,23]. On the one hand, Ω_{LI} is reduced when the gain-to-loss ratio is increased, as predicted by theory [2]. This explains why Ω_{LI} is minimum at the center frequency of the transition. However, another dependence of the lock-in threshold with frequency appears in the experimental results: The evolution of Ω_{LI} with the frequency is always asymmetric and Ω_{LI} is always smaller on the high-frequency side of the transition. This fact has never been satisfactorily explained. Besides, we now know a phenomenon that breaks the symmetry of the output-power versus frequency profiles: the resonant diffraction-losses mechanism [24]. In particular, we have shown that in the case of the usual RLG (two-isotope mixture, short cavity in both planes), the output power is always more important on the high-frequency side of the transition than on the low-frequency side [26] and that nonresonant diffraction can play an important role in the lock-in mechanism [27]. Consequently, one may wonder whether the lock-in threshold is minimum when the diffraction losses are minimum. The aim of this section is to show experimentally that the asymmetries of the lock-in versus frequency profiles are indeed correlated with the asymmetries of the output-power profiles and that the lock-in threshold is minimum on the side of the profile where the output power is maximum.

In order to study the dependence of the lock-in threshold with the laser frequency one must scan this frequency by changing the cavity length. Besides, we know that scanning the cavity length modifies the lock-in threshold for another reason. Indeed, the lock-in threshold is usually interpreted as due to the local defects of mirrors [4]. When one of the mirrors is moved, the points of incidence of the beams on the mirrors are changed and the distances between the involved residual local defects are changed. This modifies the vectorial sum of the backscattered waves [4]. The effect we are trying to observe here can consequently be hidden by these changes of the relative phase shifts between the backscattered waves. Hence we choose arbitrarily to build a "bad" RLG. We indeed choose to use very diffusing mirrors for which the position of the incidence point of the beam on mirrors will not have any influence on the lock-in threshold. We will then be able to explore the role of the frequency detuning on the lock-in threshold.

The experimental setup is schematized in Fig. 8. The

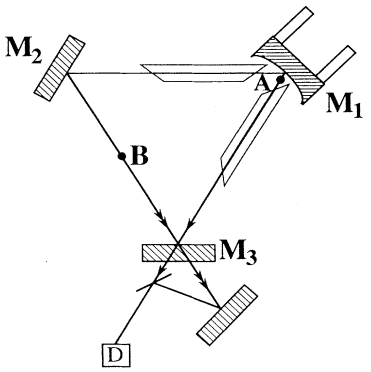

FIG. 8. Experimental setup used to observe the dependence of the lock-in threshold with the frequency detuning.

laser oscillates at $\lambda = 3.39$ μm and the cavity is equilateral with a perimeter equal to 84 cm. The spherical mirror has a radius of curvature equal to 50 cm. Two identical 12-cm-long discharge tubes are located on each side of the spherical mirror and have a 6.2-mm inner diameter, allowing one to select the saturation lenslike effects [31]. In these conditions, when the two discharge tubes are located near the spherical mirror, the cavity is long (short) in both planes when the diffracting aperture at point A is located near the spherical mirror M_1 (at point B between mirrors M_2 and M_3) [24]. Mirrors M_1 and M_2 are totally reflecting and mirror M_3 transmits 6% of the incident intensity. The use of two identical discharge tubes with the same discharge currents allows our cavity to remain symmetrical and to avoid the null-shift effects investigated in Sec. II. The two output beams are recombined in order to measure the frequency difference between the two modes. The whole setup is mounted on a rotating table with variable angular velocity and one makes sure that no null shift exists by comparing the results obtained for the two directions of rotation of the experiment.

In the first step, the discharge tubes are filled with a 5:1 ^{3}He-^{20}Ne mixture at total pressure $P = 1.1$ Torr. We first check that the saturation lenslike effect is predominant and that the cavity is short when the aperture is located at B [see Fig. 9(a)] and long when the aperture is located at point A near mirror M_1 [see Fig. 10(a)]. The experiment is then rotated and one can observe that the beating due to the Sagnac effect appears first on the low-frequency side of the transition for a short cavity [see Fig.

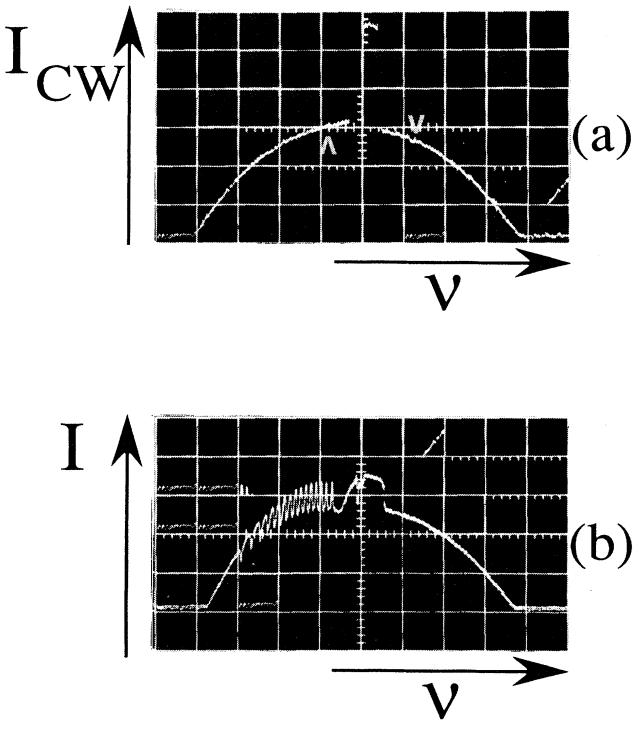

FIG. 9. Experimental results for a one-isotope RLG with a cavity that is short in both planes (horizontal axis: 30 MHz per division). (a) The RLG is at rest. Output power of the CW mode only vs frequency. The asymmetry of this profile shows that the cavity is short in both planes. (b) The RLG turns at angular frequency $\Omega = 25°/s$. The two output beams are recombined on the detector and one notices that the lock-in threshold is lower on the low-frequency side.

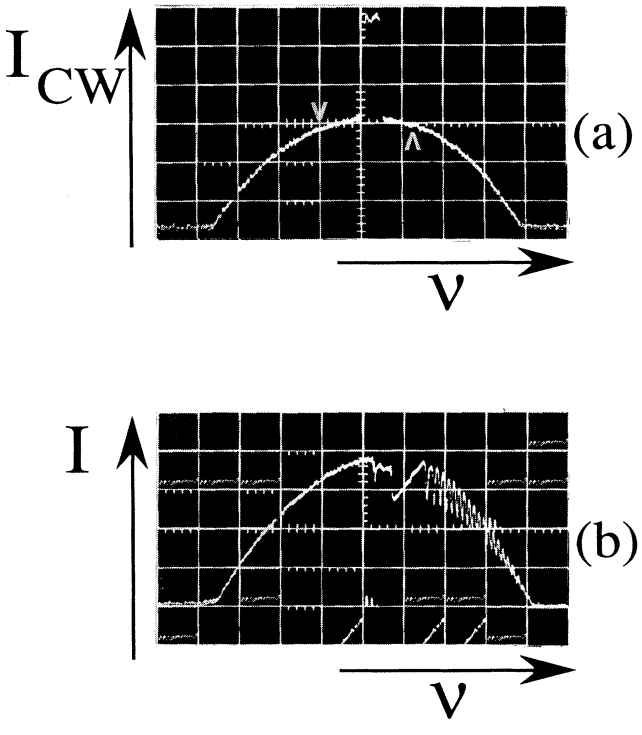

FIG. 10. Experimental results for a one-isotope RLG with a cavity that is long in both planes (horizontal axis: 30 MHz per division). (a) The RLG is at rest. Output power of the CW mode only vs frequency. The asymmetry of this profile shows that the cavity is long in both planes. (b) The RLG turns at angular frequency $\Omega = 22°/s$. The two output beams are recombined on the detector and one notices that the lock-in threshold is lower on the high-frequency side.

9(b)] and on the high-frequency side of the transition for a long cavity [see Fig. 10(b)]. The tubes are then filled with a 1:1:10 ^{20}Ne:^{22}Ne:^{3}He at $P=1.1$ Torr. At this pressure for the 3.39-μm transition, we know that the sign of the saturation lenslike effect must be the same for the two-neon-isotope mixture as for the one-neon-isotope mixture [26]. Here again the asymmetries of the output-power profiles and of the lock-in threshold profiles with respect to frequency are inverted when one passes from a short cavity (see Fig. 11) to a long cavity (see Fig. 12). In all experiments, two points are carefully checked: (i) the asymmetries of the output-power versus frequency profiles for the RLG at rest are the same for the two counterpropagating modes; and (ii) the lock-in threshold measurements give the same result for the two directions of rotation, showing the absence of any null shift.

These results show that the lock-in mechanism depends not only on nonresonant diffraction effects, as shown in Ref. [27], but also on resonant diffraction effects. *The lock-in threshold is indeed minimum where the output power is maximum,* i.e., where the diffraction losses are minimum.

IV. CONCLUSION

In conclusion, we have shown that the resonant diffraction mechanisms that are correlations between the transverse mode structure and the intensity in ring lasers [24,26] also induce correlations between the transverse-mode structure and the frequency characteristics of ring-laser gyroscopes. We have indeed shown that these resonant diffraction mechanisms have important consequences on two characteristics of the RLG: the null shift and the lock-in region. We have indeed seen that the nonreciprocity of the resonant diffraction-losses mechanism induces two different asymmetries for the two counterpropagating beams and is an important source of null shift in the RLG. The experimental results are found to be in agreement with the theoretical calculations. This allows one to justify *a posteriori* the empirical rule that states that a RLG without null shift must be symmetrical. Besides, we have seen that the resonant diffraction mechanism explains the asymmetries observed in the dependence of the lock-in threshold with the laser frequency. This explains why in the usual 6328-Å two-isotope RLG's that are built with short cavities the lock-in threshold is smaller on the high-frequency side of the transition than on the low-frequency side of the transition. These features and others [27] may have important consequence on the building of RLG cavities.

ACKNOWLEDGMENTS

The Laboratoire d'Electronique Quantique is "Unité Associée au Centre National de la Recherche Scientifique

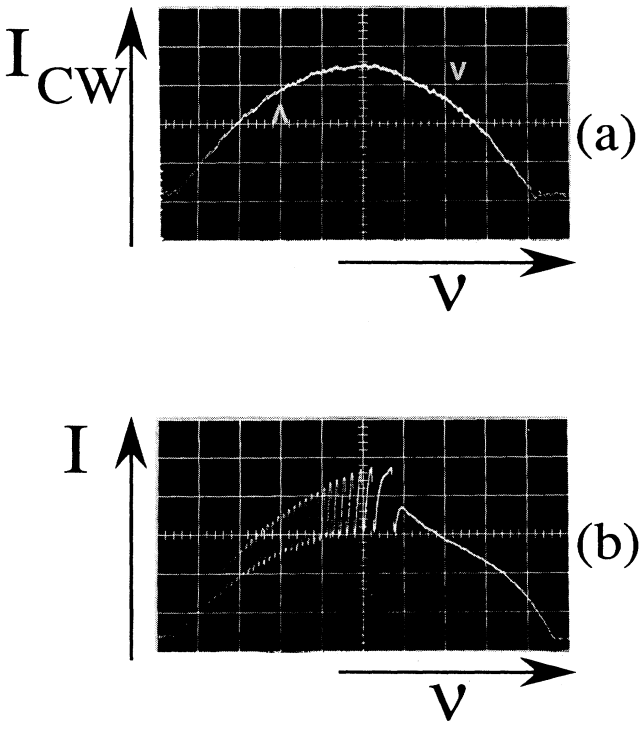

FIG. 11. Experimental results for a two-isotope RLG with a cavity that is short in both planes (horizontal axis: 30 MHz per division). (a) The RLG is at rest. Output power of the CW mode only vs frequency. The asymmetry of this profile shows that the cavity is short in both planes. (b) The RLG turns at angular frequency $\Omega=16°/s$. The two output beams are recombined on the detector and one notices that the lock-in threshold is lower on the low-frequency side.

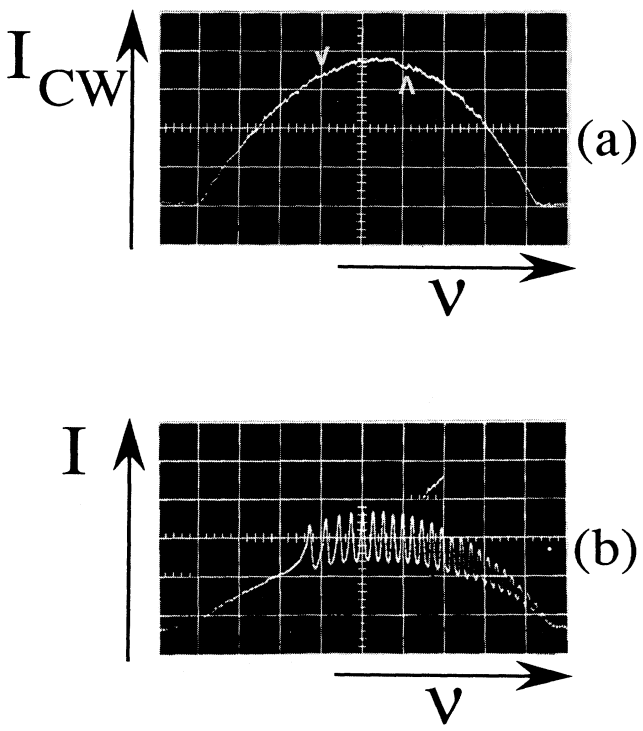

FIG. 12. Experimental results for a two-isotope RLG with a cavity that is short in both planes (horizontal axis: 30 MHz per division). (a) The RLG is at rest. Output power of the CW mode only vs frequency. The asymmetry of this profile shows that the cavity is long in both planes. (b) The RLG turns at angular frequency $\Omega=16°/s$. The two output beams are recombined on the detector and one notices that the lock-in threshold is lower on the high-frequency side.

No. 1202." This research was partially supported by the Direction des Recherches, Etudes et Techniques, the Pôle Optique and Optoélectronique de Formation des Ingénieurs par la Recherche Technologique, and the Conseil Régional de Bretagne.

APPENDIX

In this appendix we summarize the expressions of Lamb's coefficients [1] used in Eqs. (5)–(8) for the case of a two-counterpropagating-mode ring laser with a single-isotope inhomogeneously broadened active medium at third order in field. The net gain coefficients are given by

$$\alpha_{\mathrm{CW,CCW}}=F_1 \exp\left\{-\left[\frac{\omega_{ab}-\omega_{\mathrm{CW,CCW}}}{ku}\right]^2\right\} - \frac{1}{2}\frac{\omega}{Q_{\mathrm{CW,CCW}}} . \tag{A1}$$

The self- and cross-saturation coefficients are given by

$$\beta_{\mathrm{CW,CCW}}=\frac{1}{2}\frac{\gamma_{ab}}{\gamma}F_1 \exp\left\{-\left[\frac{\omega_{ab}-\omega_{\mathrm{CW,CCW}}}{ku}\right]^2\right\} , \tag{A2}$$

$$\theta_{\mathrm{CW\text{-}CCW,CCW\text{-}CW}}=\beta_{\mathrm{CW,CCW}}L(\omega_{ab}-\omega_0) . \tag{A3}$$

The linear pulling coefficients can be written

$$\sigma_{\mathrm{CW,CCW}}=-\frac{2}{\pi}\exp\left\{-\left[\frac{\omega_{\mathrm{CW,CCW}}-\omega_{ab}}{ku}\right]^2\right\} \times\int_0^{(\omega_{\mathrm{CW,CCW}}-\omega_{ab})/ku} F_1 e^{x^2}dx . \tag{A4}$$

The self- and cross-pushing coefficients are given by

$$\rho_{\mathrm{CW}}=\rho_{\mathrm{CCW}}=0 , \tag{A5}$$

$$\tau_{\mathrm{CW\text{-}CCW,CCW\text{-}CW}}=\beta_{\mathrm{CW,CCW}}\frac{\omega_{ab}-\omega_0}{\gamma}L(\omega_{ab}-\omega_0) , \tag{A6}$$

where

$$L(\omega_{ab}-\omega_0)=\frac{\gamma^2}{\gamma^2+(\omega_{ab}-\omega_0)^2} \tag{A7}$$

is the Lorentzian line shape associated with the homogeneous broadening of the transition,

$$\omega_0=\tfrac{1}{2}(\omega_{\mathrm{CW}}+\omega_{\mathrm{CCW}}) \tag{A8}$$

is the mean angular frequency for the two counterpropagating modes, and

$$F_1=\tfrac{1}{2}\omega\sqrt{\pi}\mathcal{P}^2(\hbar ku\,\varepsilon_0)^{-1}\bar{N} . \tag{A9}$$

In these expressions, $\mathcal{P}$ is the matrix element of the electric dipole, γ_a, γ_b, and γ are the relaxation rates of the levels and the optical coherences, ω_{ab} is the pulsation of the transition, ku is its Doppler width, $\gamma_{ab}=(\gamma_a+\gamma_b)/2$, $Q_{\mathrm{CW,CCW}}$ are the quality factors of the cavity, ε_0 is the dielectric permittivity of vacuum, $\bar{N}$ is the mean population inversion along the cavity length, and $\hbar$ is Planck's constant. The approximation of inhomogeneously broadened transition assumes that $ku \gg \gamma$.

*Also at Société d'Applications Générales d'Electricité et de Mécanique, 70-74 rue de la Tour-Billy, Boîte Postale 72, F-95101 Argenteuil CEDEX, France.

†Present address: Laboratoire de Spectroscopie du Solide, Université de Rennes I, Campus de Beaulieu, F-35042 Rennes CEDEX, France.

‡Permanent address: Ecole Normale Supérieure de Cachan, 61 avenue du Président Wilson, F-94230 Cachan, France.

[1] M. Sargent III, M. O. Scully, and W. E. Lamb, Jr., *Laser Physics* (Addison-Wesley, Reading, MA, 1974).

[2] F. Aronowitz, Ph.D. dissertation, New York University, 1969.

[3] F. Aronowitz, in *Laser Applications,* edited by M. Ross (Academic, New York, 1971), pp. 113–200.

[4] J. R. Wilkinson, in *Progress in Quantum Electronics* (Pergamon, Oxford, 1987), Vol. 11, p. 1.

[5] G. Sagnac, C. R. Acad. Sci (Paris) **157**, 708 (1913); **157**, 1410 (1913).

[6] T. J. Podgorski and F. Aronowitz, IEEE J. Quantum Electron. **QE-4**, 11 (1968).

[7] P. K. Cheo and C. V. Heer, Appl. Opt. **3**, 788 (1964).

[8] I. A. Andronova and I. L. Bershtein, Zh. Eksp. Teor. Fiz. **57**, 100 (1969) [Sov. Phys. JETP **30**, 58 (1970)].

[9] A. D. Valuev, S. A. Savranskii, A. F. Savushkin, and B. A. Shokin, Opt. Spektrosk. **29**, 410 (1970) [Opt. Spectrosc. (USSR) **29**, 217 (1970)].

[10] M. N. Burnashev and Y. V. Filatov, Opt. Spektrosk. **35**, 992 (1973) [Opt. Spectrosc. (USSR) **35**, 577 (1973)].

[11] E. E. Fradkin, Opt. Spektrosk. **31**, 952 (1972); **32**, 132 (1972) [Opt. Spectrosc. (USSR) **31**, 514 (1972); **32**, 65 (1972)].

[12] T. V. Guseva and E. E. Fradkin, Opt. Spektrosk. **36**, 975 (1974) [Opt. Spectrosc. (USSR) **36**, 572 (1974)].

[13] A. Y. Birman and A. F. Savushkin, Opt. Spektrosk. **37**, 317 (1974) [Opt. Spectrosc. (USSR) **37**, 181 (1974)].

[14] T. V. Radina and E. E. Fradkin, Opt. Spektrosk. **49**, 754 (1980) [Opt. Spectrosc. (USSR) **49**, 412 (1980)].

[15] E. Y. Opelukhin, T. V. Radina, and E. E. Fradkin, Opt. Spektrosk. **68**, 1358 (1990) [Opt. Spectrosc. (USSR) **68**, 797 (1990)].

[16] V. F. Boitsov, Opt. Spektrosk. **31**, 961 (1971) [Opt. Spectrosc. (USSR) **31**, 519 (1971)].

[17] V. F. Boitsov, T. A. Murina, and E. E. Fradkin, Opt. Spektrosk. **36**, 539 (1974) [Opt. Spectrosc. (USSR) **36**, 311 (1974)].

[18] V. F. Boitsov, Opt. Spektrosk. **41**, 864 (1976) [Opt. Spectrosc. (USSR) **41**, 507 (1976)].

[19] V. F. Boitsov, Opt. Spektrosk. **43**, 734 (1977) [Opt. Spectrosc. (USSR) **43**, 433 (1977)].

[20] V. F. Boitsov, Opt. Spektrosk. **57**, 270 (1984) [Opt. Spectrosc. (USSR) **57**, 163 (1984)].

[21] Y. V. Glushenko, T. V. Radina, and E. E. Fradkin, Opt. Spektrosk. **57**, 328 (1984) [Opt. Spectrosc. (USSR) **57**, 198 (1984)].
[22] H. A. Haus, H. Statz, and I. W. Smith, IEEE J. Quantum Electron. **QE-21**, 78 (1985).
[23] F. Aronowitz and R. J. Collins, J. Appl. Phys. **41**, 130 (1970).
[24] F. Bretenaker, A. Le Floch, and J. P. Taché, Phys. Rev. A **41**, 3792 (1990).
[25] H. Kogelnik, Bell Syst. Tech. J. **44**, 455 (1965).
[26] F. Bretenaker and A. Le Floch, Phys. Rev. A **42**, 5561 (1990).
[27] F. Bretenaker, J. P. Taché, and A. Le Floch, Europhys. Lett. (to be published).
[28] A. E. Siegman, *Lasers* (University Science Books, Mill Valley, CA, 1986).
[29] B. K. Garside, IEEE J. Quantum Electron. **QE-4**, 940 (1968).
[30] J. P. Taché, Thèse d'Etat, Université de Rennes I, Rennes, France, 1988 (unpublished).
[31] J. P. Taché, A. Le Floch, and R. Le Naour, Appl. Opt. **25**, 2934 (1986).
[32] K. E. Oughstun, Opt. Commun. **43**, 41 (1982).
[33] K. E. Oughstun, P. A. Slaymakar, and K. A. Bush, IEEE J. Quantum Electron. **QE-19**, 1558 (1983).
[34] M. Piché and P. A. Bélanger, IEEE J. Quantum Electron. **QE-20**, 1303 (1984).
[35] K. E. Oughstun, IEEE J. Quantum Electron. **QE-20**, 1306 (1984).
[36] E. M. Wright, D. P. O'Brien, and W. J. Firth, IEEE J. Quantum Electron. **QE-20**, 1307 (1984).